5-21-2003

Synthesis of Tin Oxide Nanocrystalline Phases Via Use of Tin (II) Halide Precursors

Hongmei Deng
Marquette University

Frank K. Lamelas
National Institute of Standards and Technology

Jeanne Hossenlopp
Marquette University, jeanne.hossenlopp@marquette.edu

Chemistry of Materials, Vol. 15, No. 12 (1 June 2003): 2429-2436. DOI.

Synthesis of Tin Oxide Nanocrystalline Phases via Use of Tin(II) Halide Precursors

Hongmei Deng
Departments of Chemistry, Marquette University, Milwaukee, Wisconsin
F. J. Lamelas
Departments of Physics, Marquette University, Milwaukee, Wisconsin
Jeanne M. Hossenlopp
Departments of Chemistry, Marquette University, Milwaukee, Wisconsin

SUBJECTS:
Oxides, Mixtures, Deposition, Physical and chemical processes, Solvents

Abstract

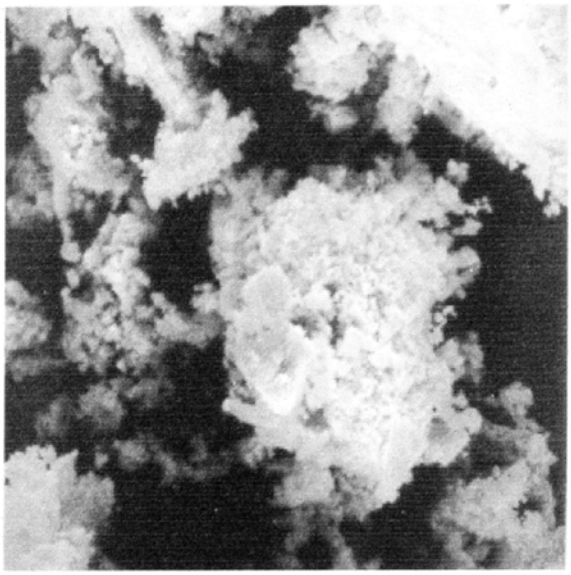

Nanocrystalline tin oxides are synthesized via precipitation from heated solutions as well as from a novel above-solution vapor deposition route that occurs at low temperatures and atmospheric pressure. Crystalline phases are characterized via powder X-ray diffraction. Samples precipitated from reactions of $SnCl_2$ are found to exist primarily as mixtures of tetragonal SnO and tetragonal SnO_2 or tetragonal SnO_2 and tin(II) oxyhydroxide ($Sn_6O_4(OH)_4$), depending on reaction conditions. A mixed tin(II)/tin(IV) sample is shown to produce a rarely observed form of the intermediate oxide Sn_3O_4 upon annealing in air at 600 °C. $SnBr_2$ exclusively forms tetragonal SnO_2 via precipitation. Variation in the solvent composition with $SnBr_2$ is shown to result in vapor deposition of SnO_2 at temperatures below 160 °C. The average crystallite sizes of the vapor-deposited material are ≈3 nm and grow slowly upon heating. Partially hydrolyzed $SnBr_4$ is proposed as the vapor deposition intermediate based on variations in precursor/solvent combinations along with FTIR and GC-MS analysis of the reaction solution removed prior to the onset of deposition.

Synopsis

The oxygen stoichiometry of nanocrystalline tin oxide powders is readily varied by controlling reaction conditions when using $SnCl_2$ as the precursor. Mixtures of SnO, SnO_2 and $Sn_6O_4(OH)_4$ are produced and a rarely observed form of Sn_3O_4 is also generated by annealing a mixed Sn(II)/Sn(IV) sample in air. Substitution of $SnBr_2$ results in exclusive formation of SnO_2, either by precipitation or by a novel low-temperature, atmospheric pressure vapor deposition route, depending on reaction conditions.

Introduction

Use of tin oxide thin films and powders in developing chemical sensors is an active field of research and numerous methods have been developed for synthesis of these materials.[1] Among the critical factors in optimizing sensor behavior of SnO_2-based materials is control of both the material grain size and the tin/oxygen stoichiometry. Grain size has been shown to influence both conductivity and sensor sensitivity with optimal sensor performance obtained when the grain diameter approaches the dimension of the charge depletion layer, ≈6 nm.[2-4]

Mixed tin oxidation states have also been suggested to influence sensor response but characterization of the specific effects has been limited to date to a few studies. Thin-film sensor response in radio frequency magnetron sputtered SnO_2 samples[2] suggests that the presence of the β-Sn phase mixed with cassiterite

SnO_2 reduces sensitivity to NO_2 and CO. Similarly, observation of the intermediate oxide, Sn_2O_3, at the interface between silicon substrates and SnO_2 films deposited via aerosol-assisted chemical vapor deposition has been proposed[5] as a potential source of sensor instability. In contrast, films containing a mixture of romarchite SnO and cassiterite SnO_2 produced via thermal oxidation of physical-vapor-deposited Sn films have been shown to be more sensitive for CH_2Cl_2 detection than either SnO or SnO_2 single-phase films.[6]

Mixed SnO/SnO_2 is intriguing as potential sensor material since p−n junctions would be expected due to the presence of the p-type SnO semiconductor along with n-type SnO_2.[7] The apparent role of p−n junctions in sensor performance of SnO_2/CuO materials has been discussed;[8] however, SnO/SnO_2 combinations for sensor applications are less well understood and controllable methods for synthesizing this mixed oxide system would be desirable. Related to this objective is the need to better understand the phase transitions that occur upon heating since SnO is not a thermodynamically stable form of tin oxide and formation of intermediate oxide forms and/or metastable Sn(II) and Sn(IV) phases may complicate characterization of the effects of tin/oxygen stoichiometry on sensor response.

Along with thermal oxidation of physical-vapor-deposited atomic tin films,[6] other reported methods for varying the stoichiometry of tin oxide materials include use of Sn(IV) and Sn(II) precursors in organometallic chemical vapor deposition,[9] as well as oxidation of the surface of thin films initially prepared by pulsed laser deposition.[10] Previous work in our laboratory[11,12] has utilized laser-assisted chemical vapor deposition (LCVD) to produce SnO_2 and doped SnO_2 films. Preliminary experiments[13] indicate that the LCVD technique can also be adapted to generate films containing polycrystalline SnO from Sn(IV) precursors. However, the desire to develop reproducible and easily controllable methods for generating mixed stoichiometry tin oxide species has motivated us to explore wet chemical approaches, such as sol−gel chemistry, that could ultimately be coupled with LCVD doping. Sol−gel approaches also provide better potential control of grain sizes. Our current efforts are thus focused on developing chemical methods for controllable stoichiometry in nanoscale tin oxide films and powders. The primary focus of this report is on the crystalline products of SnO_x powder synthesis from Sn(II) halide precursors.

Experimental Section

$SnBr_2$ (Strem), $SnCl_2$ (anhydrous 98%, Strem), $SnBr_4$ (99%, Aldrich), $SnCl_4$ (anhydrous 98%, Strem), methanol (99.93%, Aldrich), ethanol (absolute, Aaper), and 3 M ammonium hydroxide solution, NH_3−H_2O (reagent grade, Fisher), were used as supplied without further purification. Large $SnBr_2$ crystals were milled with a mortar and pestle to reduce their size prior to use.

Precipitated powder samples were synthesized in a spherical glass reactor by heating solutions containing the tin halide precursor (1.00 g of $SnBr_2$ or 0.68 g of $SnCl_2$) with varying amounts of alcohol, distilled water, and/or aqueous ammonia, until most or all of the solvent and other volatiles were distilled off via a condensor arm and solid materials were obtained. Summaries of the reaction conditions are listed in Table 1. Specific adaptations made to the published[14] SnO synthetic route include the elimination of tin powder from all reaction mixtures, substitution of $SnBr_2$ for $SnCl_2$, and variations made in the solvent composition as well as the atmosphere under which experiments were run. $SnCl_2$ or $SnBr_2$ precursors were mixed with ≈1.4 mL of methanol and then added to 100 mL of 3 M aqueous ammonia. Additional 50−100-mL aliquots of the ammonia solution were added when ≈20−30 mL of solution remained after heating; the total volume used is indicated in Table 1. When formation of dark precipitates was observed, additional distilled water was added and the mixture was heated at ≈95 °C for 1 h. After cooling, excess solvent was removed by filtration. The precipitates were washed repeatedly with distilled water and allowed to air-dry. Experiments were performed under either air or a nitrogen atmosphere. When used, N_2 was continuously bubbled through the reaction mixture starting 30 min prior to heating and continuing until the remaining sample was cooled to room temperature. In the case of the alcohol-rich solvent

mixture, 100 mL of alcohol was mixed with 6.5 mL of water and no additional solvent was used. Selected final samples were also placed in open ceramic boats and subjected to furnace annealing in air.

Table 1. Experimental Conditions and Product Identification for Key Reactions

tin precursor	solvent	atmosphere	product appearance	crystalline product(s)
$SnCl_2$	1.5 mL of methanol	N_2	black	SnO, SnO_2
	300 mL of $NH_{3\,(aq)}$			
	150 mL of H_2O			
$SnCl_2$	1.6 mL of methanol	air	green/brown	SnO, SnO_2, plus unassigned phase
	300 mL of $NH_{3\,(aq)}$			
	200 mL of H_2O			
$SnCl_2$	1.2 mL of methanol	air	yellow	SnO_2, $Sn_6O_4(OH)_4$
	500 mL of H_2O			
$SnBr_2$	1.4 mL of methanol	N_2	yellow	SnO_2
	750 mL of $NH_{3\,(aq)}$			
$SnBr_2$	100 mL of methanol[a]	air	white	[b]SnO_2
	6.5 mL of H_2O			
$SnBr_4$	100 mL of methanol	air	white	[b]SnO_2
	6.5 mL of H_2O			
$SnBr_4$	100 mL of H_2O	air	white	[b]SnO_2

[a] Similar results, but lower yield, obtained with ethanol. [b] Vapor-deposited product.

Vapor-deposited powders were synthesized by heating 1.00 g of $SnBr_2$ in a mixture of 100 mL of methanol and 6.5 mL of water (molar ratio of alcohol:H_2O = 100:1) at 66 °C in air, which resulted in the initial formation of a yellow-brown viscous solution when most of the solvent was removed. Continued heating of this material led to vapor deposition of a white solid on the inside surfaces of the reaction chamber. The vapor deposition became visually evident when the temperature, as registered by a thermometer in contact with the inside bottom surface of the reaction chamber, reached 110 °C. The temperature increased to a maximum value of ≈160 °C during the deposition process.

Variations were also made in vapor deposition reaction conditions to further characterize this process. The effects of the tin precursor oxidation state and halide identity were explored by substituting $SnBr_4$, $SnCl_2$, or $SnCl_4$ for $SnBr_2$. Solvent effects were investigated by use of ethanol in place of methanol with the $SnBr_2$ precursor and by repeating the process using $SnBr_2$ and $SnBr_4$ precursors in pure water.

X-ray diffraction (XRD) analysis of the powder samples was carried out using a Rigaku diffractometer operated in a parafocusing Bragg-Bretano configuration with a $^1/_2$° divergence slit, $^1/_2$° scatter slit, 0.15-mm receiving slit, and 0.15-mm monochromator receiving slit. The Cu source was operated at 1 kW. Data were acquired using a 0.036° step size in 2θ and, unless otherwise noted, 20 s/step integration time. Powder samples were mounted for XRD analysis on microscope slides using 10% GE 7031 varnish in ethanol or, for samples that were reactive and/or soluble in this mixture, with double-sided tape. Peak assignments were made using a powder diffraction database,[15] considering all feasible stoichiometric combinations containing Sn, O, H, Cl or Br, N, and C as potential products. The instrument response was obtained using the National Institute of Standards and Technology (NIST) standard reference material Si powder (SRM 640C). To estimate crystallite sizes and integrated peak intensities, the peaks were fit to pseudo-Voigt functions using XFIT,[16] correcting for the instrument response, background signal, and the contribution of the Cu $K\alpha_2$ wavelength. Reported uncertainties were obtained by propagating the uncertainties of fit parameters through subsequent calculations.

Scanning electron microscopy (SEM) analysis was performed on one powder sample using a JEOL JSM 35 scanning electron microscope, using the powder as collected. The residual halogen content of powders, as synthesized, was determined via elemental analysis performed by Midwest Microlab, LLC.

Fourier transform infrared (FTIR) spectroscopic analysis was performed for selected reaction mixtures prior to final product formation. Samples were heated until 10−15 mL of solution remained and then allowed to cool to room temperature. Some of the residual liquid was coated on IR cards (Janos Technology) or CaF_2 flats and spectra were acquired at 4-cm^{-1} resolution on a Nicolet 560 FTIR spectrometer. Films coated on the IR cards were dried at 40 °C while those on the CaF_2 substrates were subjected to annealing in air over a higher temperature range (up to 500 °C). Gas chromatography-mass spectrometry (GC-MS) was used to look for potential vapor deposition intermediates. A portion of the same sample prepared for the FTIR experiments was dissolved in acetone and injected into a Hewlett-Packard GC-MS.

Results and Discussion

Variations in precursor identity and/or reaction conditions led to the formation of polycrystalline materials either via precipitation or via a vapor deposition process where products were found to condense on the walls of the spherical reaction chamber *above* the solution. A summary of the key reactions is given in Table 1.

A. Precipitated Nanocrystalline Tin Oxides.

A series of adaptations to the standard literature route for SnO synthesis from $SnCl_2$ were first performed to explore the conditions that would produce mixtures of tin oxide species. The first reaction was performed under N_2 and a black precipitate was obtained. The XRD analysis of this product is shown in Figure 1A. The expected positions and relative intensities of tetragonal (romarchite) SnO are shown just below Figure 1A, confirming that the major product was SnO, consistent with the black color of the material. In addition, weak and broad features were observed in the expected positions for tetragonal (cassiterite) SnO_2 as shown in the expanded scale plot in Figure 1B. The sample used to obtain the data shown in Figure 1 was found via elemental analysis to contain 0.8 ppt Cl, although no crystalline Cl-containing phases were evident.

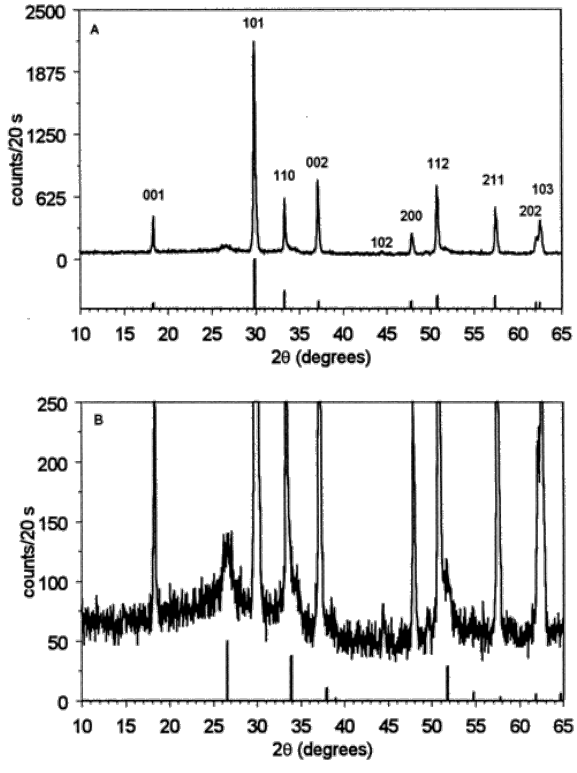

Figure 1 Powder X-ray diffraction data for precipitated products obtained from $SnCl_2$ heated under N_2 with aqueous ammonia. (A) Stick spectrum and *hkl* indexing provided for reflections assigned to the major phase, SnO [PDF# 6-0395]. (B) Expanded scale with positions and relative intensities shown for tetragonal SnO_2 [41-1445] (see Figure 5 for SnO_2*hkl* indexing).

The Scherrer equation was used, assuming a shape factor of 0.9,[17] to estimate average crystalline sizes using the SnO 101 and the SnO_2 110 reflections. The SnO crystallite size was found to be 63 ± 3 nm, while the SnO_2 phase was significantly smaller in size, 4.7 ± 0.4 nm. The ratio of the background-corrected integrated intensity of the peak corresponding to the SnO 101 reflection to the integrated intensity of the SnO_2 110 reflection is 4:1. Heating the powder sample in air at 600 °C for 2 h resulted in conversion of most of the SnO to SnO_2.

The synthesis was then repeated under air, rather than N_2, which resulted in the formation of a green-brown precipitate that contained 1.1 ppt Cl. The XRD analysis of this product is shown in Figure 2A. To more closely examine small peaks observed for this sample, the XRD data shown in Figure 2A were obtained using a 40 s/point integration time. SnO features are found in this sample (marked with triangles in Figure 2A), along with more pronounced SnO_2 features (marked with diamonds). Performing the synthesis in air led to the expected reduction in the yield of SnO and increase in that of SnO_2. When measured using a 20 s/point sampling time, the integrated intensity of the SnO 101 reflection decreased by ≈60% from that shown in Figure 1, while the SnO_2 110 reflection increased by the same percentage relative to the corresponding Figure 1 value. The ratio of the integrated intensity of the SnO 101 reflection to that of the SnO_2 110 reflection was found to be 1:1 for the data acquired under the same XRD scan settings as Figure 1. Average crystallite sizes were similar to those found previously, 48 ± 2 nm for SnO and 6.8 ± 0.6 nm for SnO_2.

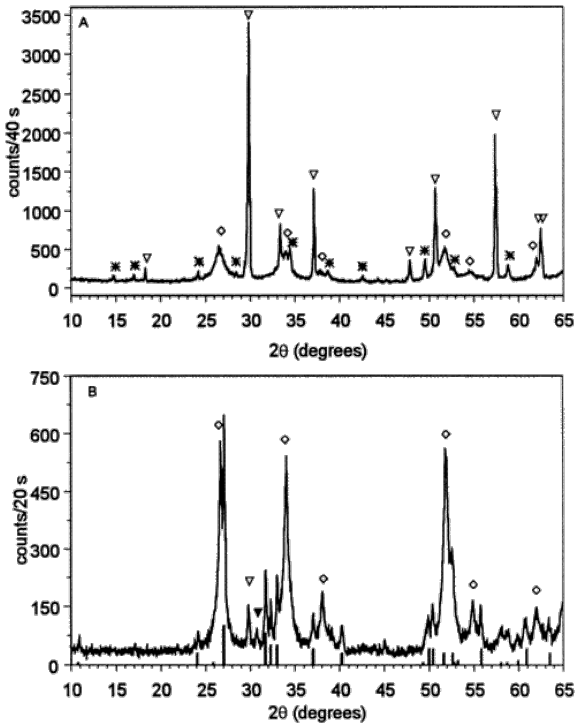

Figure 2 Powder X-ray diffraction data for precipitated products obtained from $SnCl_2$ heated under air with $NH_{3(aq)}$. (A) Powder as obtained. Open triangles indicate peaks assigned to tetragonal SnO, open diamonds indicate tetragonal SnO_2, and asterisks mark unassigned phase. (B) Powder after heating in air for 2 h at 600 °C. Open triangle indicates SnO 101 peak, open diamonds mark SnO_2 peaks, and the filled triangle indicates the position of the β-Sn 202 reflection. Positions and relative intensities for peaks assigned to Sn_3O_4 [PDF# 16-737] are shown below the data.

In addition, there is at least one more crystalline phase present; the unassigned peaks are indicated with an asterisk in Figure 2A. Along with possible Sn-containing products including the orthorhombic SnO_2 phase,[18-24] other potential crystalline impurities, including NH_4Cl and ammonium complexes of Sn(II) chloride such as $(NH_4)_2SnCl_4 \cdot H_2O$ (PDF# 27-46) and $NH_4SnCl_3 \cdot H_2O$ (PDF# 27-35), were considered in an effort to index these peaks but no satisfactory assignment was found.

To further explore the source of the minor unassigned component(s), the sample was heated at 300, 600, and 900 °C. Heating at 300 °C lowered the relative intensities of the unassigned peaks. Heating at 600 °C diminished the SnO features, increased the SnO_2 component, and produced a new set of peaks as shown in Figure 2B. Finally, we note that after the sample was heated at 900 °C, the sample color changed to yellow and only peaks assignable to tetragonal SnO_2 were present.

The new phase observed in Figure 2B after heating at 600 °C can be assigned to a form of the intermediate oxide, Sn_3O_4. A number of different intermediate oxides, $Sn_{x-1}O_x$ (x = 3, 4, and 6), have been proposed as metastable phases produced in the disproportionation of SnO as shown in reaction 1:

$$\mathrm{xSnO} \rightarrow \mathrm{Sn_{x\text{-}1}O_x} + \mathrm{Sn} \quad (1)$$

The structures, and even the existence, of the intermediate oxide phases have historically been the subject of some controversy.[25-27] A triclinic form[26] of Sn_3O_4 has been reported to be produced in SnO films heated in air[7,19] or in powders heated under N_2.[26] This same species has recently been reported in thermal annealing of SnO diskettes.[28] Sn_3O_4, but not Sn, was observed when the diskettes were heated in air at 500 °C for 2 h. Annealing the diskettes at 700 °C led to complete conversion to SnO_2. These results[28] are consistent with the multistep mechanism shown below:

$$4\mathrm{SnO_{(s)}} \rightarrow \mathrm{Sn_3O_{4(s)}} + \mathrm{Sn_{(1)}} \quad (2)$$

$$\mathrm{Sn_3O_{4(s)}} \rightarrow \mathrm{SnO_{2(s)}} + \mathrm{Sn_{(1)}} \quad (3)$$

$$\mathrm{Sn_{(1)}} + \mathrm{O_2} \rightarrow \mathrm{SnO_{2(s)}} \quad (4)$$

A different phase attributable to Sn_3O_4 has also been assigned based on a combination of XRD and Mössbauer spectroscopy.[27] This alternate form has been reported to originate from SnO samples heated under vacuum. The SnO was produced via the reaction of $SnCl_2$ with NH_4OH, similar to the route used here. Reactions 2 and 3 were proposed to explain the observed phase transitions.[27] The XRD pattern for this species is distinctly different from that indexed for the triclinic form.

The new XRD peaks that appeared in our sample when heated at 600 °C (Figure 2B) correspond to the alternate form of Sn_3O_4. The stick spectrum at the bottom of Figure 2B gives the positions and relative intensities previously reported for this phase.[27] The appearance of this phase after heating at 600 °C and conversion to SnO_2 at 900 °C is consistent with the stepwise mechanism involving reactions 2−4 and is similar to the formation of triclinic Sn_3O_4 from SnO diskettes. One peak corresponding to β-Sn is observed, but as expected for annealing in air where reaction 4 can take place, the Sn features are less evident than those assigned to the intermediate oxide.

The method of preparation of SnO and the partial pressure of O_2 present during annealing have been noted to influence the observed disproportionation/oxidization pathways. It is interesting to note that the intermediate

oxide was only observed in previous work[27] when evacuated samples containing <1% SnO_2 were heated. Our sample containing primarily SnO (Figure 1) was also heated at 600 °C in air for 2 h and no obvious evidence for the intermediate oxide was obtained. We also note that the green-brown color of the sample that generated the intermediate oxide is similar to that reported in the literature for mixed Sn(II)/Sn(IV) species.[29] The color of our sample remained unchanged after heating at either 300 or 600 °C. Further work is necessary to explore whether the unassigned minor phase initially present in this sample is directly related to the formation of intermediate oxide as well as to more fully characterize the tin oxidation states by complementary methods such as Mössbauer spectroscopy.

The third adaptation in the sequence of $SnCl_2$ reactions involved performing the synthesis in air with water rather than aqueous ammonia. This led to the formation of a mixture of SnO_2 and a second crystalline product that was assigned to be $Sn_6O_4(OH)_4$, tin(II) oxyhydroxide, as shown in Figure 3. This sample was found to contain 1.5 ppt Cl. With use of the 310 peak at 35.9°, the average size of the $Sn_6O_4(OH)_4$ phase is estimated to be 52 ± 16 nm. The tin(II) oxyhydroxide and SnO_2 mixture was also formed when aqueous ammonia was added after heating in the water/methanol mixture. Further heating, in air, of samples that contain $Sn_6O_4(OH)_4$ resulted in conversion to SnO_2 at temperatures above 300 °C.

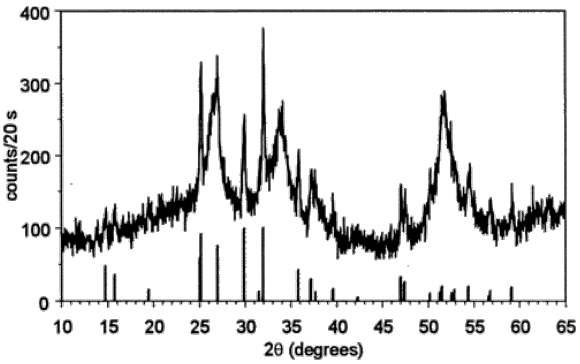

Figure 3 Powder diffraction data for precipitated sample prepared from $SnCl_2$ heated under air without aqueous NH_3. Positions and relative intensities of $Sn_6O_4(OH)_4$ peaks [PDF# 46-1486] are shown below the data.

As a final modification in this first sequence of reactions, $SnBr_2$ was substituted for $SnCl_2$. This resulted in a significant difference in product formation. Use of analogous conditions to reaction that produced predominately SnO from $SnCl_2$ (Figure 1) led to the observation of only broad characteristic features of SnO_2, as shown in Figure 4, and no residual Br was detected in this sample. The average crystallite size was estimated to be 2.5 ± 0.1 nm. No evidence for the formation of polycrystalline SnO, $Sn_6O_4(OH)_4$, or any other phase could be obtained under any conditions when $SnBr_2$ was used as the tin source. The exclusive formation of polycrystalline Sn(IV) oxide from $SnBr_2$ is consistent with periodic trends in ease of oxidation of SnX_2 by O_2.[30,31]

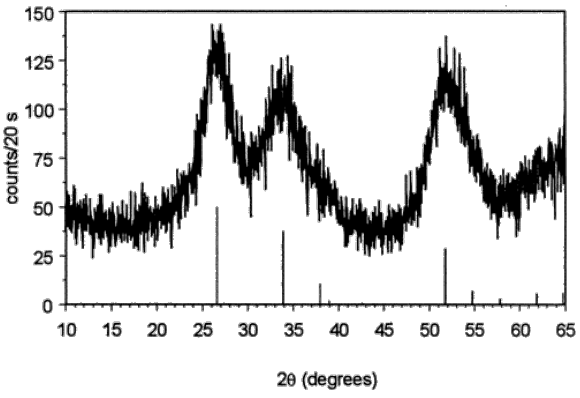

Figure 4 Powder X-ray diffraction data for precipitated products obtained from $SnBr_2$ heated under N_2 with aqueous ammonia. Positions and relative intensities of tetragonal SnO_2 are shown below.

These variations in the literature route for SnO synthesis indicate that the mixed Sn(II)/Sn(IV) oxides can be readily obtained in varying relative yields. From the perspective of potential application of this general route for synthesis of sensor materials, we do note two issues: (a) the need to more effectively remove the residual halogen, most critical in samples with larger initial crystallite sizes, and (b) the significant difference in the average crystallite sizes of the SnO and the SnO_2 products. Future work will explore variations in reaction conditions to lower the crystallite size of the SnO phase so that the influence of this parameter on sensor response can ultimately be examined.

B. Vapor-Deposited Nanocrystalline SnO_2.

Variations in the solvent composition were also attempted and an above-solution vapor deposition of nanocrystalline SnO_2 was observed under certain conditions. The XRD analysis of this product as formed is shown in Figure 5. Note that this sample was not washed as were the precipitated samples and thus contains substantially more residual Br, 59.2 ppt. The powder, as synthesized, shows broad peaks assignable to SnO_2. Heating this material in air results in the sharpening of the SnO_2 XRD peaks as also shown in Figure 5. Crystallite sizes slowly increased from ≈3 nm for the material as synthesized to 16 nm after heating at 900 °C and are summarized in Table 2. The effect of temperature on the crystallization of the vapor-deposited SnO_2 was found to be quite similar to that observed for precipitated gel/powder samples,[32,33] with very slow increases in the average crystallite size.

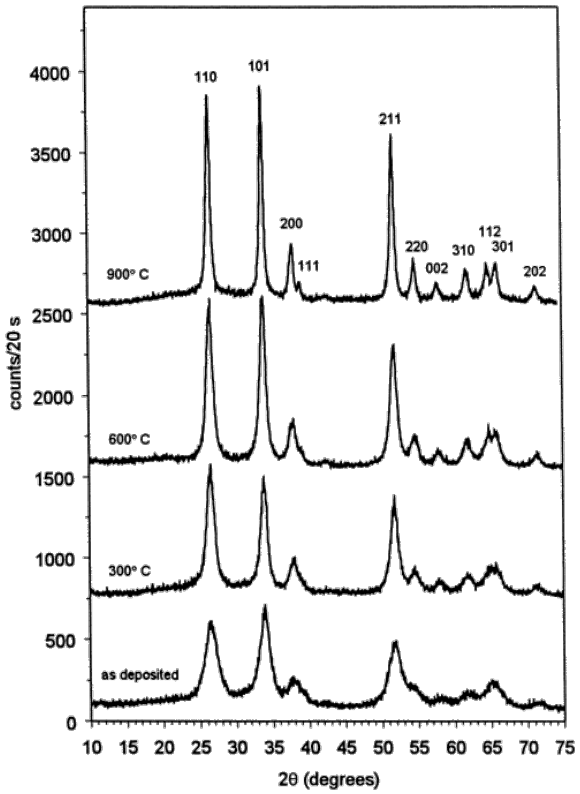

Figure 5 Powder diffraction data for vapor-deposited product. Annealing temperatures are indicated. Indexing for tetragonal SnO_2 is shown above top trace. Traces are offset for clarity but not otherwise scaled.

Table 2. Average Crystallite Size

sample	Scherrer (nm)	ε (nm)[a]	e_{rms}[a]
SnO_2 as vapor-deposited	3.1 ± 0.1	N.A.	N.A.
SnO_2, 300 °C	4.6 ± 0.1	N.A.	N.A.
SnO_2, 600 °C	7.5 ± 0.2	5.6 ± 0.7	$2(1) \times 10^{-3}$
SnO_2, 900 °C	15.5 ± 0.5	13 ± 1	$2(1) \times 10^{-3}$

[a] Uncertainties obtained from regression analysis.

Since microstrain effects also lead to peak broadening, size−strain analysis was carried out for comparison with the results obtained using the Scherrer equation. The pseudo-Voigt parameters obtained from peak fitting were used to approximate Voigt functions.[34,35]Only the data obtained at 600 and 900 °C were sufficient for strain analysis since accurate determination of the Lorentzian component of the integral breadth is more difficult in the presence of a large background.[36] Williamson-Hall analysis[37] indicated no evidence of anisotropic broadening. The apparent volume-weighted average size, ε, and rms strain, e_{rms}, were extracted from size−strain plots[38] and the results are shown in Table 2. Strain effects were found to be small contributors to the peak widths.

While the average crystallite size estimated from the XRD analysis of the as-deposited material is <5 nm, the actual particle sizes are significantly larger. The morphology of the vapor-deposited material is shown in the SEM image of Figure 6. The particles exhibit a range of sizes and have a dendrimer-like appearance at the edges. The smallest discernible structure was ≈100 nm in size. The extent of aggregation of these particles requires further investigation.

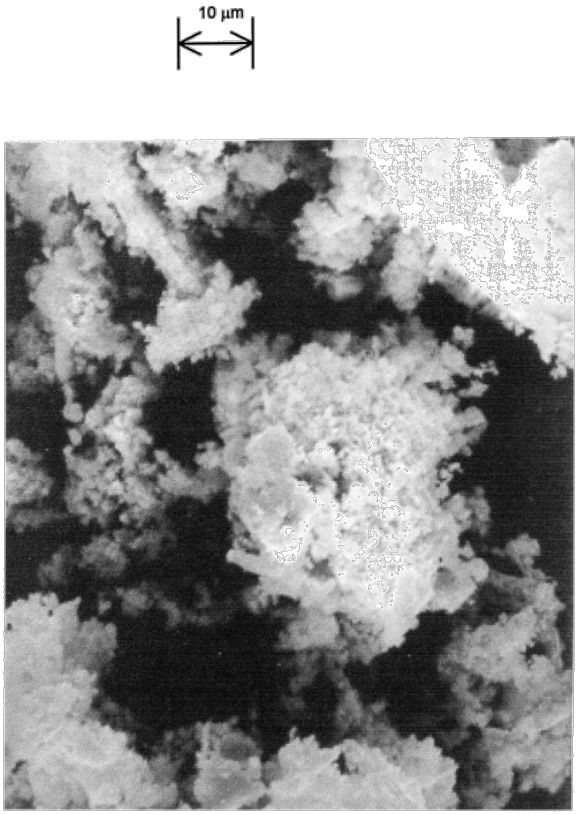

Figure 6 SEM image of vapor-deposited powder.

An additional sequence of experimental modifications was performed to determine the conditions necessary for vapor deposition. Key results are described here. Substitution of ethanol for methanol resulted in a lower yield

of the vapor-deposited product when using the $SnBr_2$ precursor. Vapor deposition was also completely suppressed when $SnBr_2$ was heated in neat methanol. $SnBr_2$ heated in pure water ultimately led to deposition of a red-brown liquid on the reaction chamber walls but did not result in the white powder. We note that $SnBr_2$ did not dissolve completely in water before the heating began. Replacing $SnBr_2$ with an equimolar quantity of $SnBr_4$ led to vapor deposition of SnO_2 from either methanol/water or pure water solvents. Finally, no vapor deposition was observed for any solvent system when $SnCl_2$ or $SnCl_4$ were used.

Vapor deposition must involve intermediates that are volatile enough to escape from the solution prior to extensive oligomerization via hydrolysis and condensation reactions. A similar phenomenon for tin sulfide films has been reported. In that case, $SnCl_2$ was heated with sulfur in solvent mixtures of carboxylic acids and water[39] and films of variable composition Sn_xS_y were observed to form above the solution−air interface beginning at a temperature of ≈60 °C. The proposed source of these films was the reaction of $SnCl_4$ condensed on the chamber walls with H_2S vapor. Similarly, $SnCl_4$ has been shown to react with H_2O to produce SnO_2 in atomic layer deposition experiments.[40]

Heating $SnBr_4$ in either water or in the mixed CH_3OH/H_2O solvent resulted in vapor-deposited product, in contrast with $SnCl_4$ where this phenomenon was not observed in the case of either solvent. This could either be due to forming different intermediates in solution or it could more simply be due to having a reaction system with an optimized temperature range for generating the vapor-deposited product from $SnBr_4$. Since $SnCl_4$ boils at 114.1 °C and $SnBr_4$ not until 202 °C,[41] the bromide precursor may reside longer on the upper walls of the reactor and thus more readily undergo reaction. However, there are also some differences in aqueous reactivity that could also contribute by generating different distributions of tin complexes. Aqueous Sn(IV) chloride and bromide solutions have been examined using ^{119}Sn NMR spectroscopy.[42] Six-coordinate haloaquostannates of the form $[SnX_y(H_2O)_{6-y}]^{4-y}$ (X = Cl or Br) were observed. The relative distribution of ligand combinations varied as a function of initial SnX_4 concentration. NMR line widths indicated that ligand exchange reactions are significantly faster for bromide ions than for chloride ions, leading to relatively more Cl complexation in the product distributions for any given SnX_4 concentration. The aqueous $SnBr_4$ solutions also exhibited NMR peaks assigned to hydrolysis products involving hydroxo-bridged Sn dimers such as $[Sn_2(\mu\text{-}OH)_2Br_4(H_2O)_2]$. These differences in complex distributions could also play a role in controlling the vapor deposition yields under our reaction conditions.

For the $SnBr_2$ precursor, vapor deposition required use of alcohol in the solvent mixture and yield was dependent on alcohol identity. A potential explanation could involve the creation of a volatile tin alkoxide or alkoxide derivative that condenses and then decomposes on the chamber walls. Hydrolytic thermal decomposition of metal alkoxides on surfaces is known to produce metal oxides from a variety of precursors,[43] including formation of SnO_2 from $Sn(OBu^t)_4$.[44] Formation of tin alkoxide intermediates has been invoked in descriptions of sol−gel syntheses of SnO_2 via heating $SnCl_2$ in methanol[45] or ethanol.[46] Given the volume of water present in the solvent mixture, any alkoxides that are present are likely to have undergone some degree of hydrolysis, possibly generating species such as $Sn(OR)_x(OH)_y$.[47]

To examine the possible contribution of alkoxide or alkoxide derivatives as intermediates when $SnBr_2$ was heated in the alcohol/water solvent mixtures, the reaction was stopped with ≈15 mL of solution left. The products thus obtained from the methanol/water solvent mixture contained a small amount of solid product and the remaining liquid material was not completely soluble in acetone. The acetone-soluble fraction exhibited a single, broad GC peak that occurred at relatively short retention times after the solvent elution and the MS features were not significantly affected by column temperature. Among the most prominent features in the mass spectrum were the characteristic cracking patterns for $SnBr_4$[48] and HBr. A small cluster of peaks centered about m/z 314 was observed, consistent with the $SnBr_2(OH)_2$ ion. Unambiguous assignment of this cluster could not be made since the weakness of the ion signals made it impossible to determine whether the full set of Sn

and Br isotopes were present. A number of other features that did not contain tin were also observed, indicating organic byproducts were also present.

FTIR spectra are shown in Figure 7 for samples of the intermediate solution coated on IR cards (7A) and CaF_2 flats (7B). Heating $SnBr_2$ in either the methanol/water or the ethanol/water solvent mixture resulted in similar spectra after drying at 40 °C, as shown in Figure 7A. Above 1900 cm^{-1}, broad absorption due to OH stretching modes is observed along with alkyl CH_x stretching features at ≈2900 cm^{-1}. The CH_x bands are more evident in the case of the ethanol solvent mixture. Key features observed below 1900 cm^{-1} include an intense band due to the water deformation mode at ≈1650 cm^{-1} and peaks at 1468, 1392, 1308, 1147, 1086, 943, 670, and 580 cm^{-1} (peak positions assigned for the ethanol solvent). For comparison, a card was coated with a 15% solution of a commercial SnO_2 sol (Alfa Aesar, 0.015-µm particles) and dried at 40 °C. The spectrum of this sample is generally less structured but contains broad features in the regions where our samples also absorb. The bands observed at 670 and 580 cm^{-1} are similar to those reported for sol−gel preparation of SnO_2,[45,49] assigned as Sn−O−Sn and Sn−O vibrations, respectively. The bands found in the 900−1300-cm^{-1} region resemble those assigned to Sn−OH modes.[50,51]

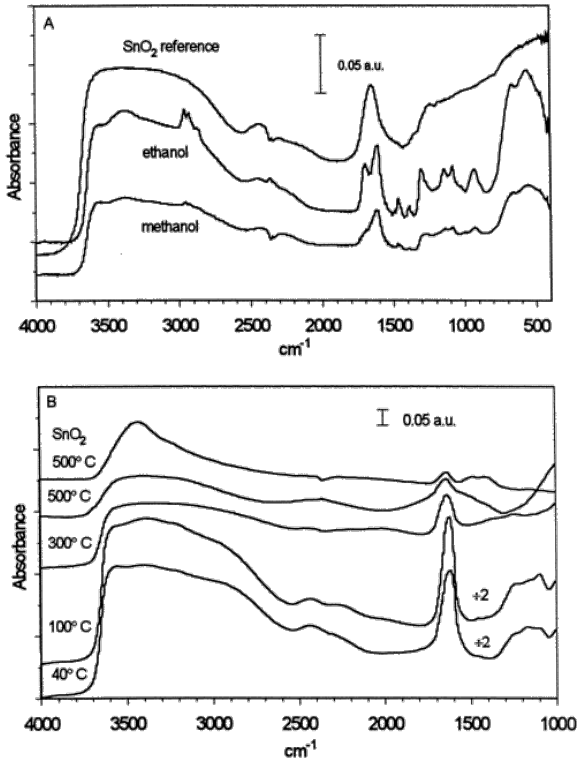

Figure 7 FTIR data for vapor deposition intermediate solutions. Samples were generated using $SnBr_2$ heated in methanol (or ethanol)/water solvent mixtures. Spectra have been offset for clarity and the scale is indicated by the 0.05 absorbance unit bar shown on each plot. (A) Samples coated on IR card and dried for 2 h at 40 °C. (B) Sample taken from methanol solvent mixture, coated on CaF_2 substrate, and annealed sequentially at the temperatures indicated. The absorbance values of the bottom two traces have been divided by 2. Upper trace shows reference SnO_2 sol heated under the same conditions.

The effects of heating were also examined to provide an additional check on the infrared assignments. The solution obtained from $SnBr_2$ heated in the methanol/water mixture was coated on a CaF_2 substrate so that the samples could be heated to higher temperatures than those feasible with the IR cards. After the samples were dried at 40 °C, the FTIR spectrum resembles that obtained with the IR card except that the peaks are broadened. The 1000−4000-cm^{-1} portion of the spectrum is shown in the lowest trace of Figure 7B. The film was

then heated for 2 h at increasing temperatures and spectra were acquired, at room temperature, between heat treatments. Little change is observed after annealing at 100 °C. After heating at 300 °C, the water deformation band is significantly decreased in intensity and the band center shifts from 1625 to 1640 cm^{-1}. Further annealing at 500 °C leads to broadening of the 1640-cm^{-1} peak with increased absorbance also observed in the 1350−1570-cm^{-1} region. A substrate was also coated with the commercial sol, diluted to 8%, and subjected to the same heating regime. The top trace of Figure 7B shows this sample after heating at 500 °C, which also exhibits absorption in the 1350−1570-cm^{-1} region when compared with lower temperature treatments. Similar structure was noted in a study of thermal dehydration of tin oxide gel and was assigned to overtones of the Sn−O−Sn modes.[50]

We also note that preliminary XRD analysis of films cast from the reaction mixtures indicate that films are initially amorphous but exhibit tetragonal SnO_2 peaks after heating to 400 °C and no other polycrystalline phases have been observed.[52] This suggests that some degree of oligomerization takes place when drying these intermediate samples, stabilizing against loss of volatile tin complexes.

Taken together, these data support the hypothesis that the most likely intermediate for the vapor deposition process is a partially hydrolyzed tin(IV) bromide species. Under the reaction conditions used here, solution-phase Sn(II) would be oxidized by oxygen to Sn(IV).[30,31,53] Noting that $SnBr_2$ did not completely dissolve in water alone, the primary role of the alcohol in the vapor deposition may simply be to enhance solubility to create the appropriate intermediates for vapor deposition. Yields of the vapor-deposition process decrease in ethanol, which may serve to form more stable tin ethoxide or ethoxide derivatives that can oligomerize, leading to precipitated products.

Future work will explore the effects of varying the substrate temperature on the nature of the deposited material as well as optimize methods, such as additional exposure to H_2O vapor, for reducing the bromine content of the material as deposited. By controlling conditions such as deposition time and substrate temperature, it should also be possible to produce thin films rather than powders. Since the crystallite size in the as-vapor-deposited sample is smaller than the estimated size of the SnO_2 charge depletion layer and can be systematically increased by heating, this process for depositing SnO_2 should provide a convenient method for exploring the effects of crystalline size on gas-sensing properties, provided that the residual Br can be reduced.

Conclusions

$SnCl_2$ is a suitable precursor for synthesis of nanocrystalline mixed Sn(II)/Sn(IV) oxide powders. A rarely observed form of Sn_3O_4 can be generated by annealing, in air, samples containing a mixture of tetragonal SnO, tetragonal SnO_2, and a minor amount of an unassigned phase. $SnBr_2$ and $SnBr_4$ can be used as precursors for an efficient low-temperature, atmospheric pressure vapor deposition of nanocrystalline SnO_2, most likely via a partially hydrolyzed Sn(IV) bromide intermediate. As vapor-deposited, the average SnO_2 crystallite size is ≈3 nm and can be increased systematically by annealing in air.

Supporting Information Available

Mass spectrum of acetone-soluble intermediates (PDF). This material is available free of charge via the Internet at http://pubs.acs.org.

Terms & Conditions

Acknowledgment

We thank J. Collins for technical support of the X-ray diffractometer, M.G. Steinmetz for assistance with the GC-MS experiments, W. E. Brower, Jr., for the SEM data, and C. Yi and M. Ryan for helpful discussions. This work was funded by the National Science Foundation (CHE-0074962).

References

1 Göpel, W.; Schierbaum, K. D. *Sensors Actuators, B*1995, *26−27*, 1.
2 Serrini, P.; Briois, V.; Horrillo, M. C.; Traverse, A.; Manes, L. *Thin Solid Films*1997, *304*, 113.
3 Xu, C.; Tamaki, J.; Miura, N.; Yamazoe, N. *Sensors Actuators, B* 1991, *3*, 147.
4 Zhang, G.; Liu, M. *Sensors Actuators, B*2000, *69*, 144.
5 Alfonso, C.; Charaï, A.; Armigliato, A.; Narducci, D. *Appl. Phys. Lett.*1996, *68*, 1207.
6 Park, S. H.; Son, Y. C.; Willis, W. S.; Suib, S. L.; Creasy, K. E. *Chem. Mater.*1998, *10*, 2389.
7 Pan, X. Q.; Fu, L. *J. Appl. Phys.*2001, *89*, 6048.
8 Maekawa, T.; Tamaki, J.; Miura, N.; Yamazoe, N. *Chem. Lett.*1991, 575.
9 Suh, S.; Hoffman, D. M.; Atagi, L. M.; Smith, D. C.; Liu, J.-R.; Chu, W.-K. *Chem.Mater.*1997, *9*, 730.
10 Lamelas, F. J.; Reid, S. A. *Phys. Rev. B*1999, *60*, 9347.
11 Simianu, V. C.; Hossenlopp, J. M. *Applied Organomet. Chem.*1997, *11*, 147.
12 Hossenlopp, J. M.; Lamelas, F. J.; Middleton, K.; Rzepiela, J. A.; Schmidt, J. D.; Zivkovic, A. *Appl. Organomet. Chem.*1998, *12*, 147.
13 Middleton, K. M. S. Thesis, Marquette University.
14 Humphrey, G. L.; O'Brien, C. J. *J. Am. Chem. Soc.*1953, *75*, 2805.
15 *Powder Diffraction File Alphabetical Indexes. Inorganic Phases.* JCPDS, International Centre for Diffraction Data: Swartmore, PA, 1999.
16 Cheary, R. W.; Coelho, A. A. Programs XFIT and FOURYA, deposited in CCP14 Powder Diffraction Library, Engineering and Physical Sciences Research Council, Daresbury Laboratory, Warrington, England. (http://www.ccp14.ac.uk/tutorial/xfit-95/xfit.htm), 1996.
17 Jenkins, R.; Synder, R. L. *Introduction to X-ray Powder Diffractometry;* Wiley: New York, 1996.
18 Liu, L.-G. *Science*1978, *199*, 422.
19 Cukrov, L. M.; McCormick, P. G.; Galatsis, K.; Wlodarski, W. *Sensors Actuators, B*2001, *77*, 491.
20 Nayral, C.; Viala, E.; Fau, P.; Senocq, F.; Jumas, J.-C.; Maisonnat, A.; Chaudret, B. *Chem.Eur. J.* 2000, *6*, 4082.
21 Huh, M.-Y.; Kim, S.-H.; Ahn, J.-P.; Park, J.-K.; Kim, B.-K. *Nanostruct. Mater.*1999, *11*, 211.
22 Shek, C. H.; Lai, J. K. L.; Lin, G. M.; Zheng, Y. F.; Liu, W. H. *J. Phys. Chem.Solids*1997, *58*, 13.
23 Lu, B.; Wang, C.; Zhang, Y. *Appl. Phys. Lett.*1997, *70*, 717.
24 Dai, Z. R.; Gole, J. L.; Stout, J. D.; Wang, Z. L. *J. Phys. Chem. B*2002, *106*, 1274.
25 Moreno, M. S.; Mercader, R. C.; Bibiloni, A. G. *J. Phys.: Condens. Matter*1992, *4*, 351.
26 Lawson, F. *Nature*1967, *215*, 955.
27 Gauzzi, F.; Verdini, B.; Maddalena, A.; Principi, G. *Inorg. Chim. Acta*1985, *104*, 1.
28 Dai, Z. R.; Pan, Z. W.; Wang, Z. L. *J. Am. Chem. Soc.*2002, *124*, 8673.
29 Donaldson, J. D.; Silver, J.; Thomas, M. J. K.; Tricker, M. J. *Mater. Sci.* 1976, *2*, 23.
30 Clark, R. J. H.; Maresca, L.; Smith, P. J. *J. Chem. Soc. A*1970, 2687.
31 Taylor, M. J. *J.Raman Spectrosc.*1989, *20*, 663.
32 Wu, N.-L.; Wu, L.-F. *J. Am. Ceram. Soc.*1999, *82*, 67.

33 Jayaraman, V.; Gnanasekar, K. I.; Prabhu, E.; Gnanasekaran, T.; Periaswami, G. *Sensors Actuators, B*1999, *55*, 147.
34 Langford, J. I. In *Defect and Microstructure Analysis by Diffraction*; Snyder, R. L., Fiala, J., Bunge, H. J., Eds.; Oxford University Press: New York, 1999; pp 59−81.
35 Keijser, Th. H. De.; Mittemeijer, E. J.; Rozendaal, H. C. F. *J. Appl. Crystallogr.*1983, *16*, 309.
36 Ida, T.; Ando, M.; Toraya, H. *J. Appl. Crystallogr.*2000, *33*, 1311.
37 Guillou, N.; Auffrédic, J. P.; Louër, D. *Powder Diffr.*1995, *10*, 236.
38 Louër, D. In *Defect and Microstructure Analysis by Diffraction*; Snyder, R. L., Fiala, J., Bunge, H. J., Eds.; Oxford University Press: New York, 1999, pp 673−697.
39 Engelken, R. D.; McCloud, H. E.; Lee, C.; Slayton, M.; Ghoreishi, H. *J.Electrochem. Soc.*1987, *134*, 2696.
40 Rosental, A.; Tarre, A.; Gerst, A.; Uustare, T.; Sammelselg, V. *Sensors Actuators, B*2001, *77*, 297.
41 *CRC Handbook of Chemistry and Physics*, 71st ed.; Lide, D. R., Ed.; CRC Press: Boca Raton, FL, 1990/91.
42 Taylor, M. J.; Coddington, J. M. *Polyhedron*1992, *11*, 1531.
43 Bradley, D. C. *Chem. Rev.*1989, *89*, 1317.
44 Houlton, D. J.; Jones, A. C.; Haycock, P. W.; Williams, E. W.; Bull, J.; Critchlow, G. W. *Chem. Vap. Deposition*1995, *1*, 26.
45 Giuntini, J. C.; Granier, W.; Zanchetta, J. V.; Taha, A. *J. Mater. Sci. Lett*. 1990, *9*, 1383.
46 Terrier, C.; Chatelon, J. P.; Berjoan, R.; Roger, J. A. *Thin Solid Films*1995, *263*, 37.
47 Chatelon, J. P.; Terrier, C.; Bernstein, E.; Berjoan, R.; Roger, J. A. *Thin Solid Films*1994, *247*, 162.
48 NIST Mass Spec Data Center, Stein, S. E. dir. IR and Mass Spectra. In *NIST Chemistry WebBook, NIST Stand. Ref. Data No. 69*; Linstrom, P. J., Mallard, W. G., Eds.; National Institute of Standards and Technology: Gaithersburg, MD, 2001 (http://webbook.nist.gov).
49 Senguttuvan, T. D.; Malhotra, L. K. *Thin Solid Films*1996, *289*, 22.
50 Harrison, P. G.; Guest, A. *J. Chem. Soc., Faraday Trans. 1*1987, *83*, 3383.
51 Hiratsuka, R. S.; Pulcinelli, S. H.; Santilli, C. V. *J. Non-Cryst. Solids*1990, *121*, 76.
52 Deng, H.; Hossenlopp, J. M. Unpublished results.
53 Cotton, F. A.; Wilkinson, G. *Advanced Inorganic Chemistry,* 5th ed.; John Wiley & Sons: New York, 1988; p 296.